Materials and Design 198 (2021) 109293

Contents lists available at ScienceDirect

Materials and Design

journal homepage: www.elsevier.com/locate/matdes

Quantification of the chemical reactivity of molten nitrate salts with heat treatable aluminum alloys

J.-P. Harvey [a,*], Shanti Singh [b], Kentaro Oishi [a], Barbara Acheson [b], Richard Turcotte [b], Daniel Pilon [a], Jonathan Lavoie [b], Bernard Grange [c]

[a] Polytechnique Montréal, Chem. Eng., Box 6079, Station Downtown, Montréal, QC, H3C 3A7, Canada
[b] Natural Resources Canada, Canmet Canadian Explosives Research Laboratory, 1 Haanel Dr., Ottawa, ON K1A 1M1, Canada
[c] Constellium Technology Center, CS 10027, 38341 Voreppe Cedex, France

HIGHLIGHTS

- No strong reaction between Al alloys and $NaNO_3$ up to 720 °C in a closed system.
- The Al-20%Mg alloy strongly reacts with $NaNO_3$ in an open system at 450 °C
- The Al—5%Li alloy reacts with $NaNO_3$ above its liquidus temperature in an open system
- The thermal decomposition of $NaNO_3$ promotes reactions with Al-based materials.
- Reaching the solidus temperature of a material during heat treatment is to be avoided.

GRAPHICAL ABSTRACT

Calculated Al—Mg phase diagram (left graph, solid black lines) and measured thermal curves (right graph) for Al-20%Mg + NaNO3 sample (grey X - ignition); Al-12%Mg + NaNO3 sample (black X - small exothermic reaction) and Alloy 2024(1.2%Mg) + NaNO3 (red X - small exothermic reaction).

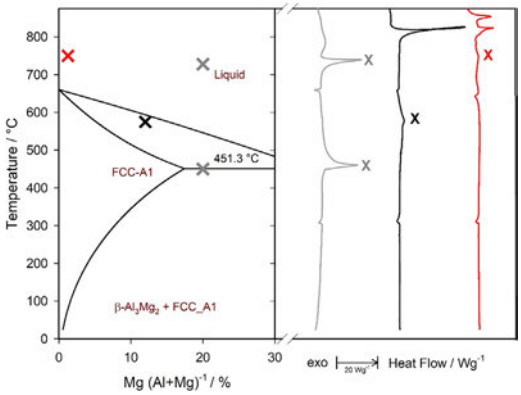

ARTICLE INFO

Article history:
Received 15 August 2020
Received in revised form 27 October 2020
Accepted 2 November 2020
Available online 5 November 2020

ABSTRACT

This work explores the conditions for safe heat treatment of aluminum alloys containing lithium and magnesium in molten sodium nitrate ($NaNO_3$) bath furnaces, and conditions where industrial accidents may occur. Using calorimetry coupled to classical thermodynamics, the strength of classical thermodynamics when analyzing thermal curves was demonstrated through a series of small-scale thermal analyses of various aluminum alloys in contact with sodium nitrate. This system was selected to illustrate reactions that may lead to severe and violent heat effect phenomena. Using idealized binary alloys, severe oxidation of magnesium- and lithium-rich aluminum alloy samples were shown to occur near 500 °C, a temperature range dangerously close to the operating temperature of solution heat treatment furnaces in manufacturing processes of heat treatable aluminum alloy sheets used in the aerospace industry. Commercial aluminum alloys AW257, 2198, 2024, and 1050 were also assessed with the same tools. The temperature that needed to be reached for these commercial aluminum alloys to react with molten sodium nitrate was significantly higher than the normal operating temperature of a conventional solution heat treatment furnace.

* Corresponding author.
E-mail address: jean-philippe.harvey@polymtl.ca (J.-P. Harvey).

https://doi.org/10.1016/j.matdes.2020.109293

1. Introduction

Aluminum alloys have been used in the automotive industry [1] and integrated into a multitude of highly technological applications in the aviation and aeronautic industries in recent years. The drive towards lighter metal alloys, mostly in military and aeronautic applications, has seen a shift from traditional aluminum-copper (2000 series), aluminum-zinc (7000 series) and aluminum-magnesium-silicon (6000 series), to aluminum-lithium compositions (2000 and 8000 series), with lithium typically added up to 2 wt% [2]. Lithium increases the specific mechanical properties of aluminum alloys (such as the specific strength) and therefore reduces their weight which is highly beneficial for aerospace applications. Multiple challenges arising from the addition of lithium into aluminum alloys are described below:

1. Fast diffusion and high mobility of lithium in the solid state that could lead to segregation at the surface of the material [3,4]
2. High reactivity and affinity with oxygen leading to lithium losses [5]
3. Decrease of the stability of the oxide layer protecting the surface of the material [3,6]

In each of these challenges, the reactivity of the lighter metals (lithium and magnesium) poses a hazard. Traditionally, molten sodium nitrate bath furnaces have been operated to process heat treatable alloys such as the 2024 alloy [7]. Aluminum alloy manufacturers are nowadays exploring the possibility of using these furnaces to process new generations of Al—Li alloys as well. In this context, ensuring a safe operation of the system is paramount. This work evaluates the reactivity of Li-containing aluminum alloys with molten sodium nitrates in the typical operating temperature range of these solution heat treatments in the industry. It also explores the usefulness of small-scale experiments to support modelling of the thermodynamic origin of such hazards. An examination of the process by which these alloys are produced is first presented, in the context of the hazards that may be present.

The practice of homogenization by heat treatment and quenching during the manufacture of heat treatable aluminum alloys is used to convey enhanced physical properties to the alloy such as strength, ductility and corrosion resistance. A typical heat treatment starts with rapid heating above the solvus temperature of the alloy, followed by quenching to achieve a supersaturated solid solution. The imposed temperature of the solution heat treatment depends on the alloy to be treated and its desired end-state properties [8] [9]. Depending upon alloy composition, the operating temperature of the furnace during a solution heat treatment can be close to a eutectic temperature but, in a real-life operation, eutectic temperatures should not be reached. However, due to micro-segregation effects induced upon non-equilibrium solidification, the chemical composition of an aluminum alloy at grain boundaries can be significantly different from that of the bulk composition. These boundaries may each have distinct eutectic temperatures, and operation of a furnace at, or above, this eutectic temperature can therefore lead to the local melting of specific regions within the alloy [10]. This must be a consideration when determining heat treatment temperatures and durations, as well as stringency of process temperature control.

Various strategies can be used to perform alloy heat treatments, such as convection furnaces or molten salt baths. Molten salts such as sodium nitrate ($NaNO_3$), potassium nitrate (KNO_3), or binary salts ($KNO_3 + NaNO_3$), as heat transfer media for aluminum alloys, have advantages over conventional heat treatment convection furnaces. As a heat transfer fluid, molten salts allow rapid heat transfer by conduction, which has been proven to be more efficient than radiant or gaseous convection furnaces [11]. Another important factor to consider when performing a solution heat treatment is the resulting deformation/distortion and dimensional defects of the treated part. Due to this, and the aforementioned micro-segregation issues, it is highly desirable to limit the time spent in the heat treatment furnace, and to limit temperature gradients in the treated part in favour of uniform heating.

Important prerequisites for the selection of molten salts for this type of application are their thermal stability and low vapour pressure in the range of working temperatures of the solution heat treatment furnaces (i.e. around 500 °C). At atmospheric pressure, $NaNO_3$ starts to thermally decompose between 500 °C to 600 °C [12] [13] depending on a number of factors including the heating rate. Under normal operating conditions, thermal decomposition of sodium nitrate is a dynamic process dependent on the atmosphere chemistry, the heating rate, the gas flow, as well as the container material [14]. The presence of impurities in nitrates such as water, cyanide or chloride can also have an important impact on their thermal decomposition behaviour (see [15] for example).

Molten nitrates are considered hazardous for multiple reasons; primarily that nitrates are oxidizers that can sustain violent exothermic reactions with combustibles which can be organic or metallic (such as in our application). Depending on the system's chemistry, this reaction can range from a simple combustion up to a detonation. As an example, the origin of an industrial explosion involving the presence of nitrate (in this case, barium nitrate) used in the synthesis of aluminum-powder-based pyrotechnical mixtures is well-documented [16]. In fact, the potential explosion hazard of such a solution heat-treatment process is predicted by classical thermodynamics. Based on these principles, a strong exothermic reaction [17] [18] [19] is thermodynamically favoured under typical operating temperature of the solution heat treatment (i.e. about 500 °C) when an aluminum alloy is in contact with a molten nitrate. In fact, classical thermodynamic calculations predict that aluminum should be oxidized by sodium nitrate even at room temperature. Kinetic constraints prevent such a catastrophic outcome and allow use of the process at an industrial scale. The presence of a dense protective oxide layer at the surface of the aluminum alloy prevents its further oxidation. Some studies [3,6] mention that reactive alloying elements such as lithium might lead to the formation of porous non-protective surface films. This could potentially promote a sustained oxidation of the aluminum alloy. This alloying element could therefore increase the risk of reaction with the molten nitrate bath. From a chemical engineering perspective, there exist mathematical criteria to predict reactor runaways such as a positive divergence linked to mass and energy balances on a segment of the reaction path [20].

Small scale experiments on the reactivity of Al—Mg and Al—Li samples submerged in pure sodium nitrate melts, performed by Clark et al. [21], are the only evidence of the potential explosive behaviour of such a process. These authors pointed out that an alloy containing more than 20 wt% Mg was required for an explosion to occur. This is well above the current amount of Mg used in commercial heat-treatable Al alloys. Interestingly, in this study explosions were recorded at temperatures as low as 450 °C, which almost perfectly matches the solidus line (melting start temperature) of the Al—Mg system. For Al—Li samples, a minimum of 5% mass Li (still higher than what is used in commercial heat treatable Al alloys) in the sample was required for the occurrence of violent exothermic reactions. The recorded explosion temperatures for the Al—Li samples were much higher, i.e. around 650 °C, which is above the liquidus line of this system. This temperature is never reached during normal solution heat treatment of aluminum alloy. However, this temperature is not too far from normal operating conditions. This implies that the temperature control and measurement is critical in this application. Failure to accurately measure the hottest spot of the heat treated aluminum alloy could potentially lead, in the worst case scenario, to an explosion.

As inferred in the above discussion, the ability to predict the conditions for runaway reactions during heat treatment (i.e., temperature, alloy composition, bath composition, etc.) is paramount to process safety and hazard prevention in any commercial development of heat-treatable alloys. The next logical step, after this risk is assessed and deemed acceptable, is to determine the effect of this heat treatment method on the evolution of the aluminum alloy part (i.e. geometrical variations of the part after quenching; lithium losses and surface segregation, etc.).

This current study provides insight to these runaway conditions through the use of experimental trials at the milligram scale combined with predictive thermodynamic modelling. A series of calorimetry experiments, performed in open and closed conditions, was used to examine various commercial and synthetic Al alloys. The synthetic Al materials contained specifically reactive alloying elements, such as lithium and magnesium, in contact with pure sodium nitrate. These two reactive elements were selected as they are added to heat treatable aluminum wrought alloys and are particularly susceptible to react with molten sodium nitrate as quantified by their standard reduction potential. Thermo-analytical methods (i.e. differential scanning calorimetry [22]) coupled with gas analyses by IR and MS were used to postulate reactions and to assess the feasibility to process lithium-containing alloys in molten nitrate bath furnaces. Comparison with thermodynamic calculations was performed to help elucidate the reaction mechanisms in these systems and to obtain a process hazards screening tool for novel Al—Li or Al—Mg alloys, at the design stage.

2. Methodology

2.1. Sample Synthesis and Preparation

All commercial aluminum alloy sheets (i.e. 1050, 2024, 6156, 2198 and AW257) were provided by Constellium. Table 1 presents the chemical analysis of each alloy, obtained by spark optical emission spectroscopy, in addition to customized Al—Mg and Al—Li binary alloys synthesized using a small-scale induction furnace (Indutherm VC 650 V). These latter samples were used to validate the experimental work of Clark et al. [21] regarding the reported explosive reaction when certain Al—Li and Al—Mg alloys were exposed to molten sodium nitrate. Reagent Plus grade $NaNO_3$ (>99.0%) and $LiNO_3$ (9.9% Li) were obtained from Sigma-Aldrich.

Circular thin section samples were punched from the alloy; chipped samples were extracted using a controlled machining procedure to limit the temperature increase below 80 °C and avoid severe oxidation of the machined chips. An example of punched and metallic chips is presented in Fig. 1. It is known that the sample procedure and preparation technique have an important impact when performing calorimetry measurement of heat treatable aluminum-alloys, as highlighted by Starink et al. [23]. In the present work, the increased surface area to mass of chips, rather than punched samples, were preferred when performing differential scanning calorimetry (DSC) tests of the alloy exposed to the molten nitrate.

2.2. Thermodynamic Calculations

Thermodynamic calculations presented in this work were performed using the FactSage software [24]. This thermochemical package has extensive thermodynamic databases for oxides, salts, metallic systems and more. These databases are used to evaluate the energetic behaviour of different stoichiometric compounds and solutions as a function of imposed intensive properties, namely temperature, pressure and molar fraction (in the case of solutions). Numerical methods and challenges associated with the identification of multiphasic equilibrium states by a constrained Gibbs free energy minimization were already presented by Harvey et al. [25].

2.3. Experimental methods

A TA Instruments 2910 DSC was used for heating closed-system experiments (pressure-tight screwed capsules that can withstand up to 100 bar) up to 720 °C, to ensure that a complete melting endotherm was captured. A purge of 50 mL min^{-1} argon, heating rate of 10 °C min^{-1} and sample masses ≤30 mg (see Table S1, supplemental material) were used. This maximum temperature is substantially higher than normal operating conditions of molten salt bath furnaces, yet may be representative of some overheating situations in industrial furnaces caused by an erroneous thermocouple reading in the system. Eutectic temperature probes are used in the industry to prevent such erroneous measurements and allow automatic shutdown of furnace heaters. A TA Instruments Q600 (SDT, simultaneous DSC/TG) was used for heating open system experiments (i.e. open crucibles for which samples can partially/fully equilibrate with the protective gas flow) to ≤1200 °C at 10 °C min^{-1}, also under 50 mL min^{-1} argon flow. Temperature, mass and heat flow calibrations of the DSC and SDT, and thermal stability measurements of the samples, were performed according to ASTM standards [26].

As the sample was heated in the SDT, the argon purge gas swept evolved gases from the sample through transfer lines maintained at 150 °C connecting the sample chamber to a FTIR (Nicolet 6700, 4 cm^{-1} resolution, 60-s spectrum acquisition time, 59 scans/spectrum). To identify additional species which are not infrared active, it proved advantageous to also couple a mass spectrometer to the SDT/FTIR to record atomic mass fragments (MS, Extrel MAX300-LG, 19 mm quadrupole MS, electron potential 100 eV, filament emission current approximately 1.5 A).

A Setaram LABSYS EVO STA with DSC measurement option (isothermal temperature accuracy of ±1 °C and 0.4 μW heat flow resolution) was also used for heating open system experiments to capture complete melting endotherms of the pure alloys without any presence of salt. Calibrations were performed as described by ASTM E794 using Sn, Pb, Zn, Al and Ag metal standards [26]. An arithmetic average of five measurements for each standard material was used for calibration. Both the calibration and sample measurements were carried out under 15 mL min^{-1} Ar atmosphere. Around 40 mg of the punched sample in a 90 μL alumina crucible (pre-annealed at

Table 1
Chemical composition of the commercial Al alloys and synthetic samples used in this work[a].

	Al[$]	Si	Fe	Cu	Mn	Mg	Zn	Ti	Zr	Li	Ag
	%mass	%mass	%mass	%mass	%mass	%mass	%mass	%mass	%mass	%mass	%mass
Commercial Alloys											
AW257–31	Balance	≤0.1	≤0.1	2.1–2.8	0.2–0.6	0.2–0.9	≤0.08	≤0.08	≤0.08	1.1–1.7	≤0.1
2198	95.282	0.029	0.038	2.96	0.009	0.335	0.008	0.032	0.145	0.914	0.256
6156	96.731	0.854	0.08	0.9	0.453	0.8	0.146	0.036	–	–	–
2024	93.8548	0.041	0.069	4.27	0.409	1.248	0.078	0.0139	0.0163	–	–
1050	99.4508	0.129	0.325	0.0022	0.044	0.034	0.009	0.006	–	–	–
Synthetic samples											
Al-12%Mg	87.5	–	–	–	–	12.5*	–	–	–	–	–
Al-20%Mg	80	–	–	–	–	20	–	–	–	–	–
Al-5%Li	95	–	–	–	–	–	–	–	–	5	–

[a] measurement presented for both alloying elements and impurities
* average of 3 measurements, last digit represents the uncertainty
$ by subtraction

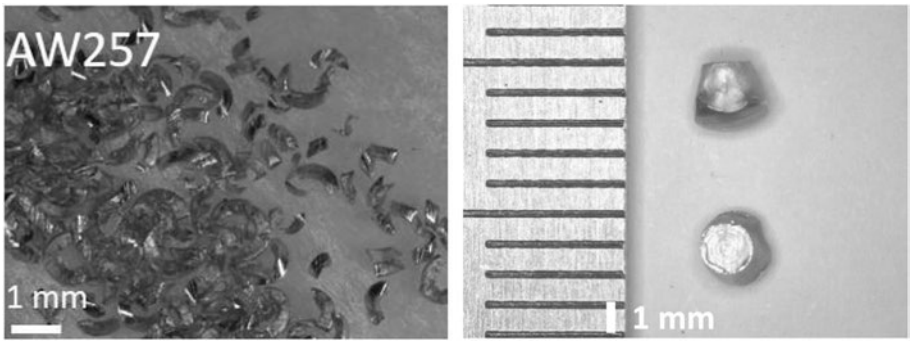

Fig. 1. Macroscopic image of Alloy AW257 metallic chips and punched samples used in the DSC tests.

1600 °C for 4 h prior to any measurement under Ar atmosphere) was placed on the DSC measurement rod. An empty and pre-annealed alumina crucible was used as reference. Both reference and sample crucibles were loosely covered with alumina lids, and a heating rate of 10 °C min^{-1} from 50 to 710 °C was applied for the sample measurements.

The limited selection of commercially available and inert closed capsules for 2910 DSC trials, and open pan materials for SDT trials led to the use of gold-sealed 316 L capsules (Netzsch Instruments Inc.) for closed system experiments and specially made INCONEL 625 pans (Instrument Specialists) for the open system experiments. It is to be noted that the closed capsules are designed so that the gold seal is not in direct contact with the molten salt or molten metal (as gold reacts with aluminum to form intermetallics), and are stated to withstand a pressure of about 10 MPa. A list of all samples tested is given in Table S1.

Consideration was given to pan selection since molten aluminum is an aggressive medium, and energetic reactions of the molten alloy and sodium nitrate has been reported by Clark [21]. Pure alumina is often recommended to contain liquid aluminum [27], however, alloying elements such as lithium and magnesium are known to rapidly degrade (shatter) Al_2O_3 crucibles because of volume mismatches induced by the formation of $LiAlO_2$ [5]. Anecdotally, when previously working with pure lithium metal in an Al_2O_3 crucible under an argon atmosphere at high temperature, a thermite-like runaway reaction was recorded during SDT calorimetry trials. This was attributed to lithium metal scavenging oxygen from the Al_2O_3 crucible. Therefore, due to the presence of lithium and magnesium in some alloy samples, metallic alloy containers were preferred, as is the case when assessing promising molten salt candidates for concentrated solar power stations and thermal energy storage system applications [28].

To assess the durability of various DSC containers in terms of metal/nitrate compatibility, a series of FactSage thermodynamic equilibrium calculations were undertaken. Specific stainless steels such as 316 alloy (austenitic steel) could be an acceptable container material [29], though stainless steel will also react to some extent with liquid aluminum [30] [31]. Others, such as ferritic steels, will be destroyed by the molten salt via different reactions such as (1) $4NaNO_3(l) + 3Fe(s) \rightarrow Fe_3O_4(s) + 4NaNO_2(l)$ or (2) $NaNO_3(l) + 3Fe(s) \rightarrow NaFeO_2(s) + Fe_2N\ (l) + 0.5O_2(g)$ [32]. The physico-chemical characteristics of a nanometric Cr_2O_3 layer are also of prime importance when looking at the corrosion behaviour of nickel alloys such as INCONEL [33]. The Cr_2O_3 layer at the surface of these materials is predicted from thermodynamics to react with liquid aluminum to form Al_2O_3. This could prevent further reaction which is one objective of Co-Continuous-Ceramic Composite materials [34]. Table 2 lists these FactSage thermochemical calculations, and other key chemical interactions, which were evaluated for standard specific enthalpy ($\Delta h°$ at atmospheric pressure) for heat interactions between the system and surroundings. These ideal data were also used for comparison to DSC thermal curves [24].

3. DSC analyses

3.1. Comparison to Model - Alloys

The correspondence between theoretical melting [24] and that recorded by DSC for the chipped and punched samples is given in Fig. 2 and Table 3. Peak melting temperature increased as the particle size increased. For each alloy sample, the lowest peak temperature corresponded to the FactSage model of idealized discrete regions of the bulk surface, which predicts thermodynamic phase equilibria based on the minimization of the Gibbs free energy of the system (which evaluation requires interpolations of binary interactions in multicomponent systems). The highest peak temperature corresponded to the punched DSC samples. Alloy 1050 is 99.45% aluminum (Table 1) and was not modelled; however, when considered as pure Al in Table 3 this alloy also followed the trend of the model resulting in a lower peak melting temperature in comparison to experiment.

The agreement between the calculated thermodynamic and experimental melting enthalpy was good, and the simulated theoretical curves also agreed with those experimentally obtained, which validated multiple aspects of our study:

1. The metallic chips and punched samples used in our tests were not too severely oxidized during the sampling procedure. As expected, the peak temperatures vary with particle size and heat transfer (Table 3). The solidus to liquidus peak temperature of each alloy was highest for the punched samples tested in an alumina cup.
2. The 316 L stainless steel was an adequate material to contain these aluminum alloys as no exothermic reactions were recorded in the 25 °C – 700 °C range.

3.2. Thermodynamic considerations

Solution heat treatments are typically performed close to the solidus temperature of the aluminum alloy. Fig. 3 shows a ternary Al-Mg-Cu isoplethal section (e.g. similar to alloy 2024 with mass fraction $X_{Mg} = 0.0125$, Table 1). Indicated on this figure is the typical solution heat treatment temperature of about 500 °C. For the 2024 alloy, this operating temperature is only 10 °C below the solidus. Therefore, if the operating temperature of the furnace is not strictly controlled it becomes probable that pre-existing chemical heterogeneities induced during manufacture of the alloy may partially melt. Fig. 4 shows the liquidus and solidus lines as well as the associated eutectic temperature for different Al-rich diagrams, covering the range of chemical compositions (for Cu, Li and Mg) listed in Table 1. Mg is the alloying element that allows the generation of a liquid phase at the lowest temperature, i.e. around 450 °C, while lithium has the highest eutectic temperature at about 600 °C. A priori knowledge obtained by modelling such alloy heterogeneities (or phases) which are susceptible to reactivity, and which exhibit a low temperature liquidus state, may allow prediction of the behaviour of the bulk when supported with small-scale tests such as DSC.

Table 2
Δh° of key phase transitions and possible chemical reactions as calculated using FactSage.

Reaction	Δh° / J g^{-1}	T / °C	Δm/m / %	Reaction Index
Melting reactions				
$NaNO_3(s) \rightarrow NaNO_3(l)$	178.5	310	0	R1
$Al(s) \rightarrow Al(l)$	397	660.3	0	R2
AW 257(solidus) → *AW 257(liquidus)*	376	[578.8–647.9]	0	R3
2024(*solidus*) → 2024(*liquidus*)	380	[507.7–642.1]	0	R4
2198(*solidus*) → 2198(*liquidus*)	377	[559.6–727.5]	0	R5
6156(*solidus*) → 6156(*liquidus*)	390	[561.8–648.8]	0	R6
Oxidation reactions (per gram of metal)				
$2Al(s) + 1.5O_2(g) \rightarrow Al_2O_3(s)$	−31,020	500	+88.9	R7
$Mg(s) + 0.5O_2(g) \rightarrow MgO(s)$	−24,710	500	+65.8	R8
$2Li(l) + 0.5O_2(g) \rightarrow Li_2O(s)$	−43,670	500	+115.3	R9
$Li(l) + Al(l) + 2NaNO_3(l) \rightarrow 2NaNO_2(l) + LiAlO_2(s)$	−146,820 (per g of Li)	700	0	R10a
$Li(l) + Al(l) + O_2(g) \rightarrow LiAlO_2(s)$	−173,065 (per g of Li)	700	+94.3	R10b
$Al(l) + 3\ Mg(l) + NaNO_3(l) \rightarrow 3MgO(s) + Na(l) + AlN\ (s)$	−23,706 (per g of Mg)	700	0	R11a
$Mg(l) + NaNO_3(l) \rightarrow MgO(s) + NaNO_2(l)$	−20,915 (per g of Mg)	700	0	R11b
Thermal decomposition reactions (per gram of $NaNO_3$)				
$NaNO_3(l) \rightarrow 0.5Na_2O(s) + 1.25O_2(g) + 0.5\ N_2(g)$	2550	750	−63.5	R12
$NaNO_3(l) \rightarrow NaNO_2(l) + 0.5O_2(g)$	1210	600	−18.8	R13
$NaNO_3(l) \rightarrow 0.5Na_2O(l) + 0.5NO_2(g) + 0.5NO(g) + 0.5O_2(g)$	3260	800	−63.5	R14
Reaction between reactants and containers (per gram of metal)				
$4NaNO_3(l) + 3Fe(s) \rightarrow Fe_3O_4(s) + 4NaNO_2(l)$	−4600 (per g of Fe)	500	0	R15
$NaNO_3(l) + 3Fe(s) \rightarrow NaFeO_2(s) + Fe_2N\ (l) + 0.5O_2(g)$	−2000 (per g of Fe)	500	−6.3	R16
$13Al(l) + 4Fe(s) \rightarrow Al_{13}Fe_4(s)$	−1870 (per g of Al)	700	0	R17
$3Al(l) + 1Ni(s) \rightarrow Al_3Ni(s)$	−2790 (per g of Al)	700	0	R18
$Cr_2O_3(s) + 2Al(l) \rightarrow Al_2O_3(s) + 2Cr(s)$	−10,723 (per g of Al)	700	0	R19
Molten salt contamination reactions				
$NaNO_3(l) + Li(l) \rightarrow LiNO_3(l) + Na(l)$	−1147 (per g of Li)	500	0	R20

3.3. Thermal decomposition of nitrates

Thermal decomposition of the nitrates was assessed first, shown in Fig. 5 for $NaNO_3$, $LiNO_3$ and a 50/50%mass ($NaNO_3$ + $LiNO_3$) mixture. $LiNO_3$ was considered since lithium may spontaneously transfer and accumulate, at a typical manufacturing operating temperature, from lithium-containing aluminum alloys into the molten salt (for example via Table 2 **R20**). In closed system tests, the maximum temperature of

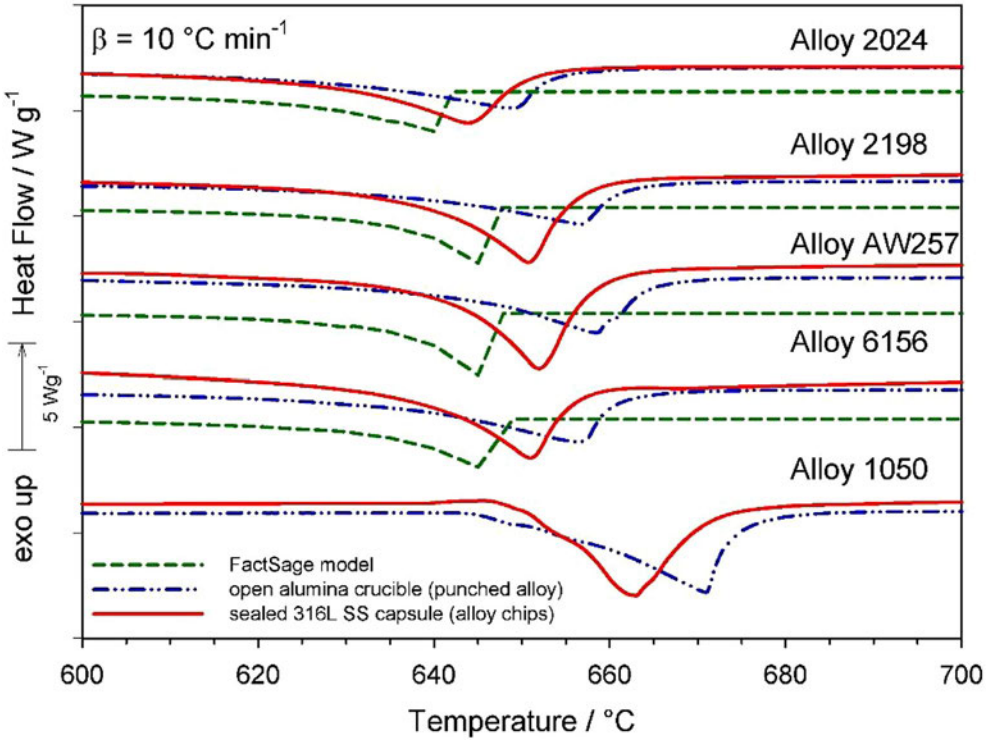

Fig. 2. Thermal curves of different aluminum alloys, displaced on the ordinate for better viewing and shown with heat flow normalized to grams of pure alloy: green long dash lines are theoretical heat flow calculated using the FactSage software, red solid lines are chipped aluminum alloys hermetically sealed in 316 L stainless capsules and blue dotted lines are punched aluminum alloys in ceramic cups.

Table 3
Theoretical vs Experimental Δh^o and peak melting temperature.

	Theoretical		*Chipped*		*Punched*	
Melting reactions	Δh^o / J g^{-1}	Tpeak / °C	†Δh^o / J g^{-1}	Tpeak / °C	†Δh^o / J g^{-1}	Tpeak / °C
$NaNO_3(s) \rightarrow NaNO_3(l)$	178.5	310	192*	307*	–	–
$Al(s) \rightarrow Al(l)$	397.5	660.3	369*	665*	339*	679*
AW 257(*solidus*) → *AW* 257(*liquidus*)	376	645	478	652	313	658
2024(*solidus*) → 2024(*liquidus*)	380	640	366	644	311	649
2198(*solidus*) → 2198(*liquidus*)	377	645	437	651	282	657
6156(*solidus*) → 6156(*liquidus*)	390	645	449	652	335	658
1050(*solidus*) → *1050*(*liquidus*)	397.5$	660.3$	356	663	344	671

* $NaNO_3$ powder and Al metal as received from supplier
$ pure Aluminum
† approximate experimental values dependent on factors such as DSC integration parameters, sample homogeneity, container heat transfer etc.

720 °C was not high enough to allow the sodium or lithium nitrate to decompose. However, under open conditions (with no pressure build-up affecting the chemical equilibrium and mass balances that are shifting because of the constantly evacuated gas phase), $LiNO_3$ and $NaNO_3$ decomposition shifted to lower temperature and each individual melting endotherm was followed by endothermic decomposition. A mixture of 50/50%mass ($NaNO_3$ + $LiNO_3$) showed a completely miscible melt having one broad endothermic peak. This recorded peak is in excellent agreement with the eutectic temperature of 194.6 °C calculated using the *FTsalt* database of the FactSage software. A decomposition endotherm occurred with mass loss starting slightly earlier than either of the pure components. This may suggest that any gradual lithium transfer occurring from the aluminum alloy to the molten sodium nitrate bath, as a function of time in real-life operation, may serve to decrease the thermal stability of the bath, relative to a pure $NaNO_3$ bath. Such a lithium transfer in the molten salt may occur via reaction R20 (Table 2) which is thermodynamically favoured under standard conditions in this range of temperature.

The first important point validated was whether thermal decomposition of the molten sodium nitrate bath was necessary for an exothermic reaction to commence within the alloy. In this scenario, the multiple chemical reactions occurring during the thermal decomposition of molten sodium nitrate, Table 2 (**R12–14**), liberate species (O_2, NO_2, $NaNO_2$, NO), which allow oxidation to promote decomposition of the alloy. The thermodynamics and kinetics of the thermal decomposition of sodium nitrate are well documented [12] [35–39]. Fig. 6 shows the FTIR and MS analyses of the evolved gases produced by thermal decomposition of the 50/50%mass ($NaNO_3$ + $LiNO_3$) during the open pan SDT measurement. The detection of both NO and NO_2 peak around 625 °C on the FTIR curve which, combined with the oxygen signal on the MS curve (mass fragment = 16), favours the decomposition mechanism defined by reaction **R14** (which is in agreement with previous

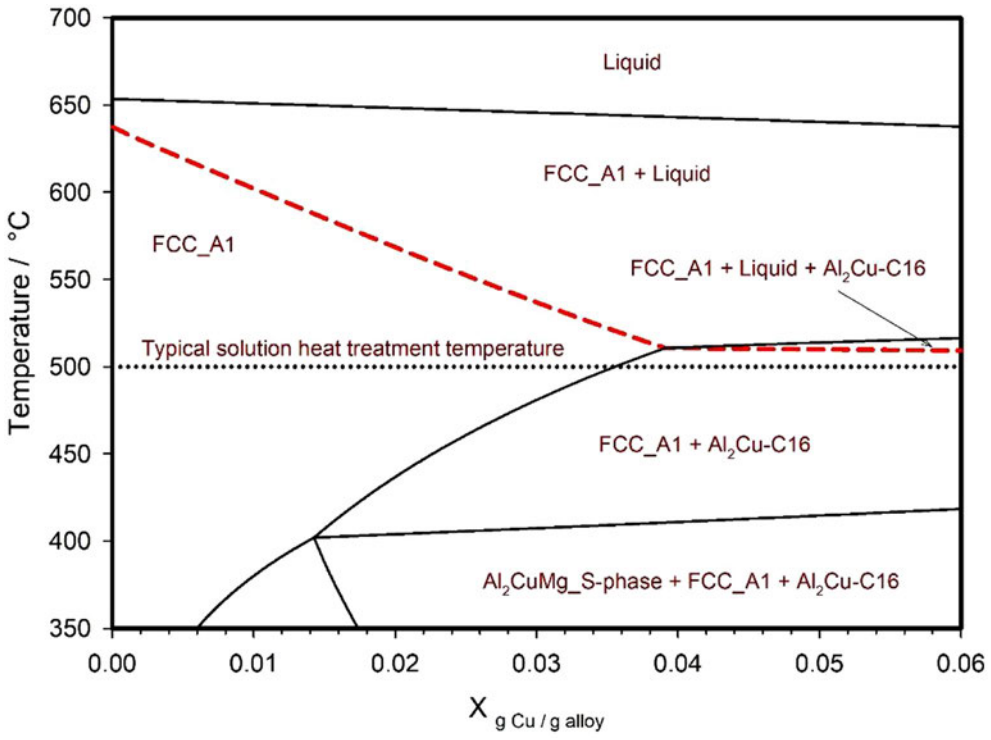

Fig. 3. Calculated Al-Mg-Cu Isoplethal section with X_{Mg} = 0.0125, 1 atm using the *FTlite* database of the FactSage software. The dashed red line represents the solidus line while the dotted line defines a typical solution heat treatment temperature for a 2024 alloy.

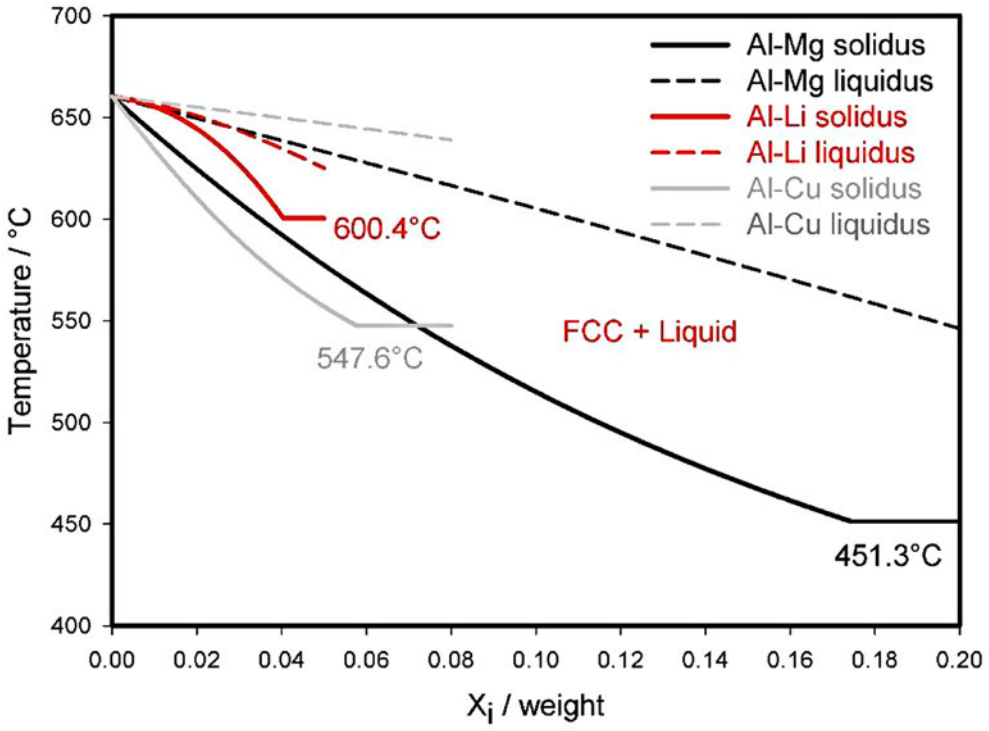

Fig. 4. Binary liquidus and solidus lines for Al-X systems as calculated by the FactSage software.

studies [14]). In this open pan configuration, the start of decomposition occurs nearly 100 °C lower than the peak temperature. Since pre-existing chemical heterogeneities induced during manufacture of the alloy may partially melt in the region above 500 °C (indicated in Figs. 3 and 4), reactive species being liberated near this temperature region would contribute to severe oxidation (including corrosion and passivation) of the aluminum alloy.

4. Reaction of alloy samples with sodium nitrate

Synthetic Al—Mg and Al—Li samples were assessed on the small scale (milligrams) to explore conditions similar to the one used by Clark et al. [21] in which very high reactivity, including explosions, were reported on the gram scale between molten sodium nitrate and aluminum alloys. Table 1 lists two samples: Al-20%Mg and Al-5%Li,

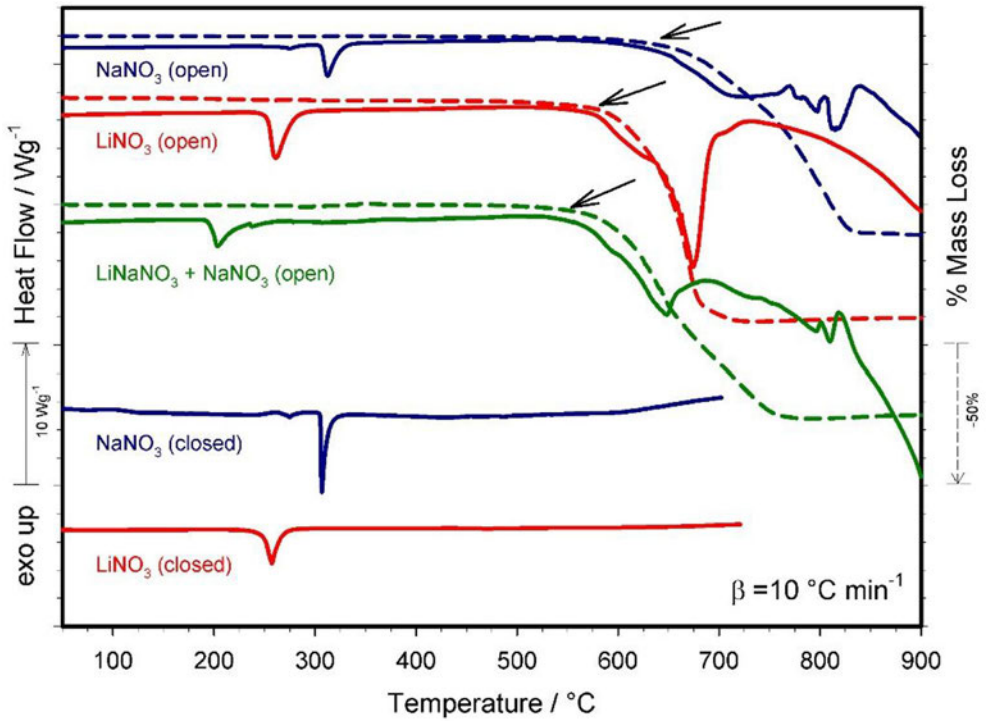

Fig. 5. DSC and SDT experiments on different nitrates in open (SDT) and closed (DSC) conditions. Mass loss indicated with dashed line and arrow pointing to onset of mass loss. All curves are displaced on ordinate for comparison.

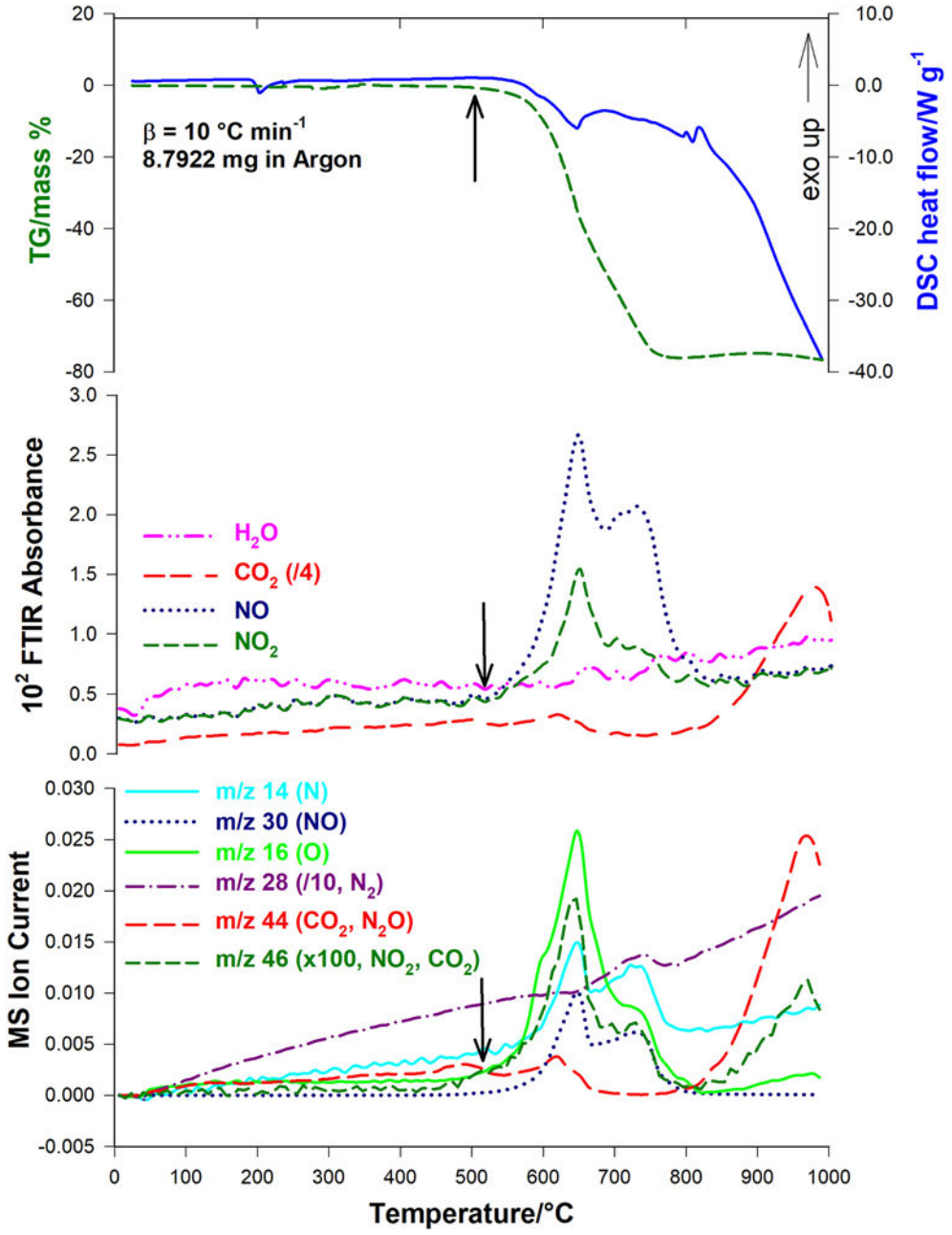

Fig. 6. DSC/TG/FTIR/MS analyses of the 50/50%mass $LiNO_3$ + $NaNO_3$ sample, with legends indicating multiple gas species where appropriate. Arrows point to onset of mass loss indicating decomposition and evolution of gaseous species.

representing compositions for which explosions were recorded by Clark et al. [21], and a third sample: Al-12%Mg, which was not identified as a strongly reactive material when exposed to molten sodium nitrate. Commercial alloys AW257 and 2198 listed in Table 1 contained both Li and Mg, and alloy 2024 contained the highest content of magnesium of the remaining samples. Each of these six samples were combined with $NaNO_3$ and assessed by calorimetry for reaction behaviour between the nitrate and each alloy on the milligram scale (Figs. 7–9).

5. Reaction of Al-Mg binary alloys

This section explores the chemical reactivity of Mg-rich synthetic samples. Their high Mg content is not representative of typical commercial Al—Mg alloys. For some of these compositions explosions have been reported in the past when exposed to a molten sodium nitrate bath. We needed to confirm these observations using our methodology.

5.1. Reaction of Al-12%Mg

Under both open and closed conditions, the Al-12%Mg sample in contact with molten sodium nitrate underwent a first small exothermic reaction between 500 and 600 °C, which may indicate a surface alloy reaction had occurred before melting of the alloy (Fig. 7, marked with 'X' on SDT thermal curve). At this temperature range, the Al-12%Mg sample was modelled to be in a 2-phase (Al-FCC + liquid) equilibrium (Fig. 8). The main exothermic reaction for this sample occurred above 800 °C (Fig. 7), a temperature which is substantially higher than both the liquidus temperature of the alloy as well as the thermal decomposition temperature of the salt. It is also well above the conventional heat

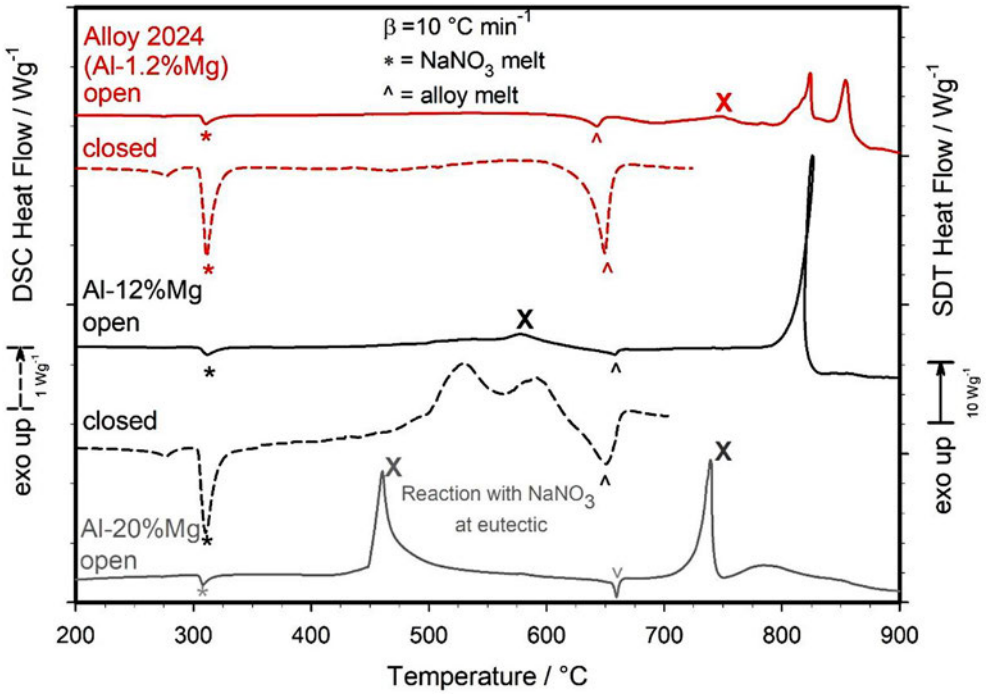

Fig. 7. Thermal curves (in W per g of mixture) of Al—Mg alloy + $NaNO_3$ in closed capsule DSC experiments up to 720 °C (dashed lines), and open pan SDT experiments up to 1000 °C (solid lines). "X" indicates discussion points in text reproduced in Fig. 8.

treatment temperature of these alloys. At this temperature, heat generated by the sample decomposition out-ran the SDT programmed sample heating rate (10 °C min^{-1}). The recorded value of SDT heatflow approached 1000 mW in the region where programmed tracking was exceeded, and such high heat flow is indicative of a runaway reaction. At this high temperature, the presence of fuels (Mg and Al) and oxidizers can be considered a reactive pyrotechnic mixture in which substantial heat was evolved due to metal oxidation [40]. Here, response

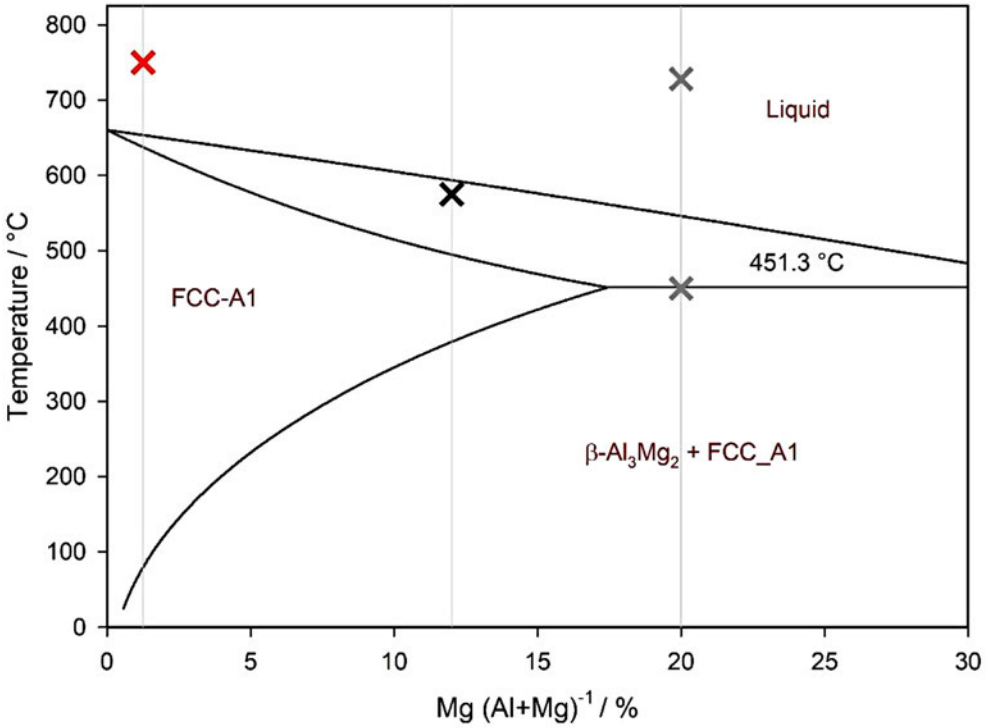

Fig. 8. Calculated Al—Mg phase diagram (solid black lines) and measured DSC exothermic reactions temperatures (X) for Al-20%Mg + $NaNO_3$ sample (grey X's - ignitions); Al-12% Mg + $NaNO_3$ sample (black X - small exothermic reaction) and Alloy 2024(1.2%Mg) + $NaNO_3$ (red X - small exothermic reaction).

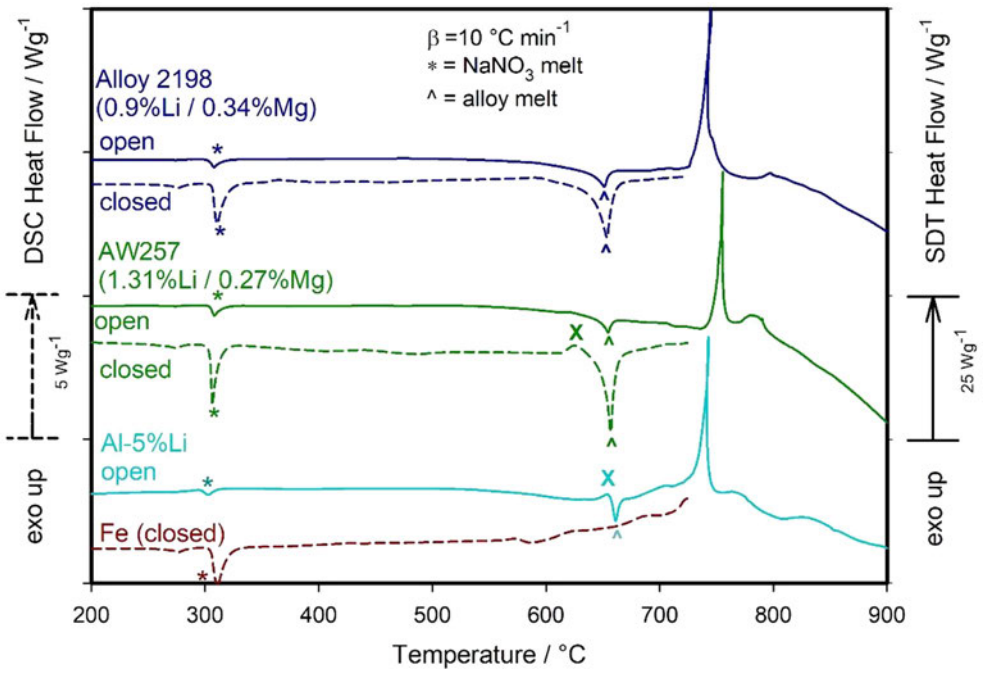

Fig. 9. Thermal curves of Al—Li alloys and Fe samples, with $NaNO_3$, in closed capsule DSC experiments up to 720 °C (dashed lines), and open pan SDT experiments up to 1000 °C (solid lines). "X" indicates discussion points in text.

of the SDT is non-ideal and the instrument's sensors could even be damaged. Indeed, thermal stability by ASTM methods [26] recommend test conditions which maintain heat flow reactions <8 mW, and require a linear heating rate to accurately determine onset to decomposition temperature (and mass loss).

5.2. Reaction of Al-20%Mg

Increasing the amount of magnesium to 20%mass greatly increased the susceptibility of the Al/Mg binary alloy to react with $NaNO_3$ as seen in Fig. 7. At first, a clear and strong exothermic signal (>2700 J g^{-1}) was recorded at 450 °C, which coincides with the eutectic temperature in the Al-rich region of this binary phase diagram (Fig. 8). The enthalpy change for this DSC exotherm (Δh^0) was estimated by integration of the associated peak in Fig. 7, which as a first approximation does not factor in heat exchange with DSC environment such as heat loss to the inert purge gas [22]. The strong exothermic signal is in perfect agreement with the observations of Clark et al. [21]. According to their observations, an explosion occurred when the metallic system reached a eutectic reaction (a 3-phase reaction). The Al-12%Mg sample described above was not rich enough in Mg to reach the eutectic reaction. This shows that the metal needs to melt to promote the rapid exothermic reaction with the molten salt. Another striking element of the Al-20%Mg system is the negligible weight loss of the sample at the first (eutectic) exothermic reaction temperature (supplemental material). This temperature is not high enough for the molten sodium nitrate to generate reactive (gaseous) thermal decomposition products with mass loss, implying that the reaction proceeded directly between the molten salt and the available metallic Al-20%Mg. Table 2 provides different reaction mechanism scenarios (see reactions R11a and R11b) that do not involve any mass fluctuation. Based on enthalpies, this exothermic reaction (449 °C, $-\Delta h \sim 2700$ J g^{-1}) had consumed a sizeable amount of the oxidizer and alloy species (Mg and Al fuel) at the eutectic reaction temperature, and as a result an ignition-type behaviour was not recorded at the higher decomposition temperature after alloy melt (729 °C, $-\Delta h \sim 1400$ J g^{-1}). Although an ignition-type behaviour was not observed, it should be noted that the starting SDT sample mass (Table S1) had been reduced by ~80% compared to the mass of (Al-12%Mg + $NaNO_3$) to reduce the chance of damage to the instrument by ignition after melting. As for the Al-12%Mg, the formation of a liquid metallic phase is required for this reaction to occur. Under normal heat treatment conditions, the formation of such a liquid phase should never occur. The range of temperature between the solvus and the solidus of a given material therefore acts as a safety factor.

6. Reaction of Alloy 2024

In the presence of $NaNO_3$ the commercial alloy 2024, containing 1.2% Mg, resulted in two exothermic events occurring after alloy melt. The start of this reaction driven by the thermal decomposition of the molten sodium nitrate to produce O_2(g) is marked with "X" in Fig. 7, indicating a small and broad exotherm with peak at 750 °C. This was followed by major molten metal oxidation peaks with total enthalpy ~1000 J g^{-1}. As with the Al-12%Mg alloy, the 2024 commercial alloy contained far less Mg than required to reach the eutectic reaction. The small exotherm was located well away from the eutectic reaction as indicated in the simplified (binary) Al—Mg phase diagram of Fig. 8. This commercial alloy can be safely solution heat treated as a reaction with the salt only occurs well after the alloy completely melted.

7. Reaction of Al-5%Li and Other Commercial Alloys

Thermal curves of $NaNO_3$ and the lithium-containing alloy samples (alloy 2198, alloy AW257 and Al-5%Li) are presented in Fig. 9. For the Al-5%Li + $NaNO_3$ (10 mg) system, there occurred a first small exothermic reaction as a shoulder before complete melting of the binary alloy (indicated with "X" on Fig. 9), in a temperature region where decomposition products linked to $NaNO_3$ are present. This sample did not show behaviour similar to the ignition reported by Clark et al. [21], contrary to the Al-20%Mg sample. The reaction kinetics for the Al-5%Li system may be influenced by the small Li atomic radius. Lithium is a fast-diffusing element that can be transferred to the molten salt, depleting Li within the aluminum alloy while producing metallic liquid sodium. Therefore, the metal-to-salt ratio may become a determining factor for

the reaction mechanism when the molten salt is in intimate contact with the aluminum alloy. The specific enthalpy of the lithium transfer reaction (Table 2, **R20**) was calculated to be significantly less exothermic than the direct lithium oxidation by $O_2(g)$ (Table 2, **R9**), which supports these observations. However, direct lithium oxidation cannot be ruled out as it may be kinetically limited. The main experimental exothermic reaction was recorded at a temperature of 750 °C, which was well above the melt temperature of the alloy, and again this behaviour appeared to be pyrotechnic-like ignition in the SDT configuration (heatflow >1000 mW). According to our results, this alloy could be safely heat treated in a molten sodium nitrate bath furnace even with this high lithium content.

The reactivity of commercial aluminum alloys, 2198 and AW257, in contact with molten sodium nitrate in closed capsule measurements did not show any strong exothermic reaction up to a temperature of 700 °C. Again, similar to the Al-5%Li system, a small exothermic event occurred prior to the melting of the AW257 alloy at around 625 °C (indicated with "X" on Fig. 9). This validates the experimental observations of Clarke et al. [21], which concluded that magnesium and lithium content of commercial alloys should be low enough to prevent severe oxidation caused by the formation of a substantial amount of liquid phase when reaching a eutectic reaction.

This figure also shows that pure iron starts to react with $NaNO_3$ (see the exothermic reactions **R15** and **R16**) above a temperature of 600 °C. In the open pan experiments of 2198 + $NaNO_3$ (15 mg) and AW257 + $NaNO_3$ (9 mg), a temperature of approximately 750 °C was required before any major decomposition exotherm occurred. Again, in this high temperature zone, reactive $NaNO_3$ decomposition products would provide oxidative species, and these samples showed pyrotechnic-like ignition behaviour in the SDT configuration. Table 2 provides the specific enthalpy of the reaction involving Al(l), Li(l) and $O_2(g)$ that leads to the formation of the highly stable $LiAlO_2$ oxide (reaction **R10b**). At this temperature, the lithium-containing alloy is fully melted while the sodium nitrate has thermally decomposed to liberate $O_2(g)$ and $NO_x(g)$. When compared to a conventional solution heat treatment of aluminum alloys, this would be about 250 °C above any normal operating temperature. Obviously, these reactions are not available for commercial alloy samples not containing Li (alloys 6156 and 1050, see Table 1). In these samples, it is expected that, similar to the Al-12%Mg system, the Mg content will not be sufficient to reach the eutectic reaction, and additionally the magnesium content of these commercial alloys should be low enough to prevent severe oxidation caused by the formation of a substantial amount of liquid phase when (or if) reaching a eutectic reaction. Although $NaNO_3$ with alloys 6156 or 1050 were not tested using SDT, it is expected that in the temperature zone above alloy melting, the molten Al and Mg would serve as fuels which would also undergo a pyrotechnic-like ignition reaction in the SDT. According to these results, it can be concluded that all these commercial alloys are chemically inert to the molten sodium nitrate bath in normal operating conditions (i.e. when the heat treated alloy stays in the solid state). These results also show that even in the eventuality that partial/local melting of the alloy occurs (because of an erroneous temperature reading of the alloy/bath), it would still require a temperature well above the liquidus of the alloy to reach strong exothermic reactions.

8. Concluding remarks

The main objective of this work was to determine whether it is safe or not to operate a molten sodium nitrate bath furnace to solution heat treat the next generation of Al—Li alloys. Under stable and fully controlled solution heat treatment temperatures (i.e. above the solvus and below the solidus), it has been demonstrated that there is virtually no reaction occurring in the system at the microscale. This is a perfect example where kinetics prevents strong exothermic reactions while classical thermodynamics predicts spontaneous oxidation of the alloy by the molten sodium nitrate.

The series of DSC analyses performed in this work also confirmed the usefulness of small-scale experiments to elucidate reactions at a large-scale, which may lead to violent heat effect phenomena. While the idealized magnesium- and lithium-rich aluminum samples (Al-12%Mg, Al-20%Mg and Al-5%Li) are not in commercial use, the 20% Mg sample clearly demonstrated that severe oxidation reactions could occur in a temperature range below the alloy melt temperature and dangerously close to the operating temperature of solution heat treatment furnaces. On the same experimental scale, oxidation was observed in the idealized 12%Mg and 5%Li samples only after the alloy melt, which is normally well above the operating temperature of solution heat treatment furnaces.

The strength of classical thermodynamics when analyzing thermal curves was also demonstrated. In fact, coupling of thermodynamic calculations with these DSC experiments and FTIR/MS gas analyses appears to be a powerful tool to understand the basic reaction mechanisms that occur in such complex systems.

As for the chemical reactivity of the commercial aluminum alloys in contact with molten sodium nitrate, our findings are consistent with the observations of Clarke et al. [21]. The temperature that needs to be reached for the commercial aluminum alloys to react with the molten sodium nitrate is significantly higher than the normal operating temperature of a conventional solution heat treatment furnace. Therefore, temperature excursions inside the solution heat treatment furnace need to be uncontrollably large to be the most evident origin of a catastrophic failure for the alloys that were studied.

Our results can also be presented in a broader context as corrosion of alloys (containers, pipes, etc.) by molten nitrate salts are among the main issues in the field of concentrated solar power plants. If the operating temperature of the molten nitrate salt in these heat storage technologies is below the solidus of these aluminum alloy, our results show that they would be chemically inert [41] [42] [43] [44].

The conclusions of our work should be taken with great care when transposed to industrial applications [18] [19]. On the scale of testing we performed, even though strong oxidation reactions were not reported within the operating temperature range of conventional solution heat treatment for lithium containing commercial alloys, we cannot claim that this operation would be without any risk at the industrial scale. A complete evaluation of the actual risks of fires or explosions for this type of molten salt furnaces would require a combined modelling of the kinetics as well as the heat dissipation rate from the heat treatment furnace. Kinetic studies could be used to generate the rate determining parameters. Quantification of the heat transfer dynamics of the furnace with its surrounding would allow to the evaluation of the temperature increase of the system upon these exothermic events. We would therefore require the following more realistic conditions in future experiments:

1. Work with dynamic operating conditions to mimic the convection movement of the molten salt in the furnace.
2. Use unaltered aluminum alloy sheets to study the influence of their metallurgical state on the reactions with the molten salt.
3. Select an adequate metal-to-salt ratio to mimic industrial conditions (to reproduce the actual lithium transfer in the molten sodium nitrate and its impact on the thermal stability of the bath).
4. Add some impurities in the molten salt bath such as water, HCl and carbonates.
5. Study the effect of long isothermal conditions on the stability of the system.

These conditions will be studied in the next phase of our work on the identification of the safety issues associated with molten salt solution heat treatment furnaces used in the aluminum industry. We also want to explore in this next phase the effect of this solution heat treatment and subsequent quenching on the quality and integrity of the heat treated Al—Li alloys to confirm the possibility to use this process at the industrial scale.

CRediT authorship contribution statement

J.-P. Harvey: Conceptualization, Methodology, Validation, Formal analysis, Writing - original draft, Writing - review & editing, Supervision, Funding acquisition. **Shanti Singh:** Methodology, Validation, Formal analysis, Investigation, Writing - original draft, Writing - review & editing. **Kentaro Oishi:** Methodology, Validation, Formal analysis, Investigation, Writing - review & editing. **Barbara Acheson:** Methodology, Validation, Formal analysis, Investigation, Writing - review & editing. **Richard Turcotte:** Methodology, Validation, Formal analysis, Investigation, Writing - original draft, Writing - review & editing. **Daniel Pilon:** Methodology, Resources. **Jonathan Lavoie:** Methodology, Validation, Formal analysis, Investigation, Writing - original draft, Writing - review & editing. **Bernard Grange:** Resources, Writing - review & editing, Conceptualization.

Declaration of Competing Interest

Bernard Grange, from *Constellium*, works on the elaboration of commercial alloys that are heat treated in molten salt furnaces.

Appendix A. Supplementary data

Supplementary data to this article can be found online at https://doi.org/10.1016/j.matdes.2020.109293.

References

[1] A. Poznak, D. Freiberg, P. Sanders, in: R. N. Lumley (Ed.), Fundamentals of Aluminium Metallurgy, Woodhead Publishing Series in Metals and Surface Engineering, Woodhead Publishing, 2018, pp. 333–386. URL: http://www.sciencedirect.com/science/article/pii/B9780081020630000102. https://doi.org/10.1016/B978-0-08-102063-0.00010-2.

[2] A. A. El-Aty, Y. Xu, X. Guo, S.-H. Zhang, Y. Ma, D. Chen, Journal of Advanced Research 10 (2018) 49–67. http://www.sciencedirect.com/science/article/pii/S2090123217301315. https://doi.org/10.1016/j.jare.2017.12.004.

[3] M. S. Udyavar, E. S. Dwarakadasa, Journal of Materials Science Letters 11 (1992) 490–492. https://doi.org/10.1007/BF00731114.

[4] U. Ramamurty, A. Bandyopadhyay, E. Dwarakadasa, J Mater Sci 28 (1993) 6340, https://doi.org/10.1007/BF01352194.

[5] N. Akhtar, W. Akhtar, S.J. Wu, International Journal of Cast Metals Research 28 (2015) 1–8, https://doi.org/10.1179/1743133614Y.0000000134.

[6] M. Ahmad, Metallurgical and Materials Transactions A 18 (1987) 681–689, https://doi.org/10.1007/BF02649484.

[7] ASM Handbook, Volume 4: Heat Treating ASM Handbook Committee, p 841–879 https://doi.org/10.1361/asmhba0001205

[8] G. Mówka-Nowotnik, J. Sieniawski, Journal of Materials Processing Technology 162–163 (2005) 367–372. http://www.sciencedirect.com/science/article/pii/S0924013605002207. https://doi.org/10.1016/j.jmatprotec.2005.02.115, aMPT/AMME05.

[9] K. Chen, H. Liu, Z. Zhang, S. Li, R. I. Todd, Journal of Materials Processing Technology 142 (2003) 190–196. http://www.sciencedirect.com/science/article/pii/S0924013603005971. https://doi.org/10.1016/S0924-0136(03)00597-1.

[10] S. Hegde, R. Kearsey, J. Beddoes, Materials Science and Engineering: A 527 (2010) 5528–5538, URL http://www.sciencedirect.com/science/article/pii/S0921509310005319, https://doi.org/10.1016/j.msea.2010.05.019.

[11] J. Laird, W. James in: Steel Heat Treating Technologies, ASM International, 2014.10.31399/asm.hb.v04b.a0005929. arXiv:https://dl.asminternational.org//chapter-pdf/289879/a0005929.pdf.

[12] P. Gimenez, S. Fereres, Energy Procedia, 69, International Conference on Concentrating Solar Power and Chemical Energy Systems, SolarPACES 2014, 2015 654–662, http://www.sciencedirect.com/science/article/pii/S1876610215003811https://doi.org/10.1016/j.egypro.2015.03.075.

[13] R.D. Scheele, J.L. Sobolik, R.L. Sell, L.L. Burger, Organic Tank Safety Project: Preliminary Results of Energetics and Thermal Behavior Studies of Model Organic Nitrate and/or Nitrite Mixtures and a Simulated Organic PNL-10213, Richland, Washington, Pacific Northwest Laboratory, 1995.

[14] T. Bauer, N. Pfleger, D. Laing, W.-D. Steinmann, M. Eck, S. Kaesche, in: F. Lantelme, H. Groult (Eds.), Molten Salts Chemistry, Elsevier, Oxford 2013, pp. 415–438, http://www.sciencedirect.com/science/article/pii/B9780123985385000202, https://doi.org/10.1016/B978-0-12-398538-5.00020-2.

[15] G. S. Picard, T. A. Flament, B. L. Trémillon, Journal of The Electrochemical Society, 132 (1985) 863–868: http://jes.ecsdl.org/content/132/4/863.abstract. https://doi.org/10.1149/1.2113974. arXiv:http://jes.ecsdl.org/content/132/4/863.full.pdf+html.

[16] M. Demichela, Journal of Hazardous Materials 148 (2007) 241–252, http://www.sciencedirect.com/science/article/pii/S0304389407002609, https://doi.org/10.1016/j.jhazmat.2007.02.041.

[17] UNECE UN Model Regulations: UN Recommendations on the Transport of Dangerous Good: Manual of Tests and Criteria, 7th revised edition, United Nations, New York and Geneva, ST/SG/AC.10/11/Rev.7, https://digitallibrary.un.org/record/3846833?ln=en 2019 (accessed 26 Oct, 2020).web.

[18] A.H. Heemskerk, A.C. Hordijk, A.T. Lanning, J.C. Lont, H. Schell, P. Schuurman, Guidelines for Chemical Reactivity Evaluation and Application to Process Design, American Institute of Chemical Engineers - Center for Chemical Process Safety, New York, 1995.

[19] R.W. Johnson, S.W. Rudy, S.D. Unwin, Essential Practices for Managing Chemical Reactivity Hazards, American Institute of Chemical Engineers - Center for Chemical Process Safety, New York, 2003.

[20] J.M. Zaldívar, J. Cano, M.A. Alós, J. Sempere, R. Nomen, D. Lister, G. Maschio, T. Obertopp, E.D. Gilles, J. Bosch, F. Strozzi, A general criterion to define runaway limits in chemical reactors, J. Loss Prev. Process Ind. 16 (3) (2003) 187–200.

[21] E. Clark, P. Gillespie, F. Page, Ins. Metals volume 3 (1986) 159–163.

[22] G. Höhne, W. Hemminger, H.-J. Flammersheim, Differential Scanning Calorimetry: an Introduction for Practitioners, Springer-Verlag Berlin Heidelberg, Germany, 1996.

[23] M. Starink, A. Hobson, P. Gregson, Scripta Materialia 34 (1996) 1711–1716 http://www.sciencedirect.com/science/article/pii/135964629600036X, https://doi.org/10.1016/1359-6462(96)00036-X.

[24] C. Bale, E. Bélisle, P. Chartrand, S. Decterov, G. Eriksson, A. Gheribi, K. Hack, I.-H. Jung, Y.-B. Kang, J. Melancon, A. Pelton, S. Petersen, C. Robelin, J. Sangster, P. Spencer, M.-A. V. Ende, Calphad 54 (2016) 35–53 , URL http://www.sciencedirect.com/science/article/pii/S0364591616300694, https://doi.org/10.1016/j.calphad.2016.05.002.

[25] J.-P. Harvey, G. Eriksson, D. Orban, P. Chartrand, American Journal of Science 313 (2013) 199–241. http://www.ajsonline.org/content/313/3/199.abstract. https://doi.org/10.2475/03.2013.02. arXiv:http://www.ajsonline.org/content/313/3/199.full.pdf+html.

[26] (a) ASTM E537–12 "Standard Test Method for the Thermal Stability of Chemicals by Differential Scanning Calorimetry" (b) ASTM E794–06(RA18) "Standard Test Method for Melting And Crystallization Temperatures By Thermal Analysis" (c) ASTM E2550–17 "Standard Test Method for Thermal Stability by Thermogravimetry" (d) E2040–19 Standard Test Method for Mass Scale Calibration of Thermogravimetric Analyzers (e) E1582–17 Standard Test Method for Temperature Calibration of Thermogravimetric Analyzers

[27] M. Yan, Z. Fan, Journal of Materials Science 36 (2001) 285–295, https://doi.org/10.1023/A:1004843621542.

[28] B. Daguanno, K.M.A. Grace, A. Floris, Scientific Reports 8, 2018, https://doi.org/10.1038/s41598-018-28641-1.

[29] Á.G. Fernández, L.F. Cabeza, 194, Solar Energy Materials and Solar Cells (2019) 160–165, URL http://www.sciencedirect.com/science/article/pii/S0927024819300789, https://doi.org/10.1016/j.solmat.2019.02.012.

[30] E. A. Carrera, J. H. Ramírez-Ramírez, F. A. Pérez-González, J. A. González, I. Crespo, Braceras, I. M. De-La Pera, A. Larrañaga, N. F. G.-M. de Oca, A. J. Pérez-Unzueta, J. Talamantes-Silva, J. L. Cavazos, R. Colás, International Journal of Cast Metals Research 30 (2017) 171–179. https://doi.org/10.1080/13640461.2017.1283878. arXiv: https://doi.org/10.1080/13640461.2017.1283878.

[31] X. Zhang, X. Li, W. Chen, Surface and Interface Analysis 47 (2015) 648–656 https://onlinelibrary.wiley.com/doi/abs/10.1002/sia.5760. doi:https://doi.org/10.1002/sia.5760.arXiv: https://onlinelibrary.wiley.com/doi/pdf/10.1002/sia.5760.

[32] A. M. Kruizenga, D. D. Gill, M. E. LaFord (2013). https://doi.org/10.2172/1104752.

[33] L. Kumar, R. Venkataramani, M. Sundararaman, P. Mukhopadhyay, S.P. Garg, Oxidation of Metals 45 (1996) 221–244 , URL https://doi.org/10.1007/BF01046827.

[34] J. Wojewoda-Budka, N. Sobczak, B. Onderka, J. Morgiel, R. Nowak, Journal of Materials Science 45 (2010) 2042–2050, https://doi.org/10.1007/s10853-009-4135-y.

[35] Y. Hoshino, T. Utsunomiya, O. Abe, Bulletin of the Chemical Society of Japan 54 (1981) 1385–1391 , URL https://doi.org/10.1246/bcsj.54.1385.

[36] E.S. Freeman, The Journal of Physical Chemistry 60 (1956) 1487–1493 , URL https://doi.org/10.1021/j150545a005.

[37] V.A. Sotz, A. Bonk, J. Forstner, T. Bauer, Thermochimica Acta 678 (2019) 178301 , URL http://www.sciencedirect.com/science/article/pii/S0040603118309894, https://doi.org/10.1016/j.tca.2019.178301.

[38] L.A. Medard, Accidental explosions, Vol 2 "Types of Explosive Substances" (p 405), Ellis Horwood Ltd, Chichester, 1989 (English Translation), ISBN10: 0745804365.

[39] A.K. Galwey, M.E. Brown, "Studies in physical and theoretical chemistry 86: Thermal Decomposition of Ionic Solids" Chapter 14.4 (p 390), Elsevier, 1999 ISBN 0-444-82437-5.

[40] J.A. Conkling, "Chemistry of Pyrotechnics. Basic Principles and Theory", MARCEL DEKKER, INC., Chapter 7 (p 145) New York, New York, 1985 ISBN 0-8247-7443-4.

[41] A. Bonk, S. Salvatore, N. Uranga, M. Hernaiz, T. Bauer, Prog. Energy Combust. Sci. 67 (2018) 69–87, https://doi.org/10.1016/j.pecs.2018.02.002.

[42] J. Gasia, L. Miró, L.F. Cabeza, Renew. Sust. Energ. Rev. 75 (2017) 1320–1338, https://doi.org/10.1016/j.rser.2016.11.119.

[43] A.G. Fernandez, B. Munoz-Sánchez, J. Nieto-Maestre, A. García-Romero, Renew. Energy 130 (2019) 902–909, https://doi.org/10.1016/j.renene.2018.07.018.

[44] W. Dinga, A. Bonka, T. Bauer, Front. Chem. Sci. Eng. 12 (2018) 564–576, https://doi.org/10.1007/s11705-018-1720-0.